RESEARCH ARTICLE

Optimized structure, Topology, Hirshfeld surface and Molecular docking analysis of some Pregnane derivatives

Neha Kumari, Rajni Kant*

Chemical Crystallography Laboratory, Department of Physics, University of Jammu, Jammu Tawi- 180006, Jammu & Kashmir, India

ABSTRACT: Pregnane, 17β- ethylandrostane, a C_{21} crystalline steroid, is indirectly a parent of progesterone. Its derivatives show some interesting biological properties. Thus, an attempt has been made to identify a few structures from the CSD database (version: 2023) for their detailed crystallographic and computational analysis. The X-ray structures have been compared with their corresponding optimized structures. Theoretical analysis of each structure has been carried out using HOMO – LUMO, MESP, Hirshfeld surfaces, crystal voids, ELF, LOL, and molecular docking. The HOMO–LUMO energy gap indicates that all structures are chemically stable. The Hirshfeld surface highlights the presence of C–H…O and O–H…O intermolecular interactions. The crystal void analysis showed that the 2α-hydroxy-5α-pregnane-3,6,20-trione molecule exhibits good mechanical stability. The molecular docking with the target protein Estrogen Receptor Beta (1qkm) reveals that 5β,6β-Epoxy-20-oxopregnan-3β-yl acetate, on the basis of its better binding score, may be a potential candidate for anti-cancer activity.

KEYWORDS: Steroids, hydrogen bonding, density functional theory, Hirshfeld surfaces, fingerprint plots, molecular docking

https://doi.org/10.29294/IJASE.11.3.2025.4120-4130

1. INTRODUCTION

Pregnanes are a subclass of steroids consisting of four-ring structure and an acetyl group attached at the C_{17} position. It serves as a parent hydrocarbon for two classes of steroids, stemming from 5α-pregnane (originally allopregnane) and 5β-pregnane, respectively. The pregnane derivatives exhibit biological properties, viz., cytotoxic, anti-cancer, anti-oxidant, anti-inflammatory, anti-asthmatic and anti-viral, etc [1-6] and have also garnered significant attention, especially in areas such as hormonal regulation, reproductive functions, cancer research and structural biology [7,8]. Breast cancer, the second most common occurring phenomenon amongst women, and the ongoing challenge in diagnosing and treating breast cancer highlights the need for new mechanism and drugs to improve patient outcomes. Research suggests that Estrogen Receptor Beta (ERβ) plays a crucial role in mediating estrogen's effects on diverse physiological processes such as cell proliferation, differentiation, inflammation, and neuroprotection [9-11].

In view of the fact that pregnane derivatives possess immense potential in the field of pharmaceuticals, we have identified a set of four such structures from the Cambridge Structural Database [CSD, *version 2023*] which are labeled as: M(a) BIZPAC (5β,6β-Epoxy-20-oxopregnan-3β-yl acetate), M(b) HXPRDO (3α-Hydroxy-5α-pregnane-11,20-dione), M(c) LOSKAG (3β,1β,14α-Trihydroxypregnan-20-one) and M(d) RAFSAU (2α-hydroxy-5α-pregnane-3,6,20-trione), respectively [12-15]. An attempt has been made to compare the X-ray structure of each derivative with its optimized geometry and also to include an analysis of HOMO–LUMO, MESP, electron localization function (ELF), local orbital locator (LOL), Hirshfeld surface (HS), 2-D fingerprint plots (FP) and crystal voids. Beside this, the molecular docking studies of each molecule with ERβ have been performed.

2. Computational details

The optimized geometry of each structure **[M(a-d)]** has been obtained using density

***Corresponding Author: rkant.ju@gmail.com**

Received: 15.01.2025 **Accepted:** 15.03.2025 **Published on**: 29.03.2025

functional theory (DFT), with three-parameter hybrid functional B3LYP and the 6-311 ++G (d,p) basis set employing the Gaussian09 software [16-18]. The individual ring conformation analysis for all the four structures has been carried out with asymmetry parameter computation. The HOMO–LUMO and MESP maps have been made using the DFT-optimized output file. The ELF and LOL plots were generated using the *.fchk file* in the Multiwfn software [19]. The Hirshfeld surfaces (d_{norm}, shape-index, 2-D fingerprint plots and crystal voids) have been generated for each molecule using Crystal Explorer 21.5 software [20], with input files having the *.cif* format.

AutoDock Vina software has been employed for the molecular docking analysis [21]. The target protein of interest is the Estrogen Receptor Beta (PDB ID: 1qkm) which served as a common protein for all pregnane derivatives. The *.pdb* file of protein 1qkm was downloaded from the RCSB Protein Data Bank (http://www.rcsb.org). Thus, using the AutoDock Tools (ADT) program, *.pdbqt* files were prepared for the protein, ligand and the standard drug molecule. The specific coordinates (X= 8.0, Y= 4.0, and Z= -2.0) were defined as the center of the grid for the identification of the active protein site. The interactions between the ligand and the protein were analyzed using the Discovery Studio 4.1 Visualizer software [22].

3. RESULT AND DISCUSSION

3.1 Crystallographic analysis

The chemical structure of each molecule is shown in Figure 1a. The chemical formula, CCDC code, cell parameters and some related crystallographic data are given in Table 1.

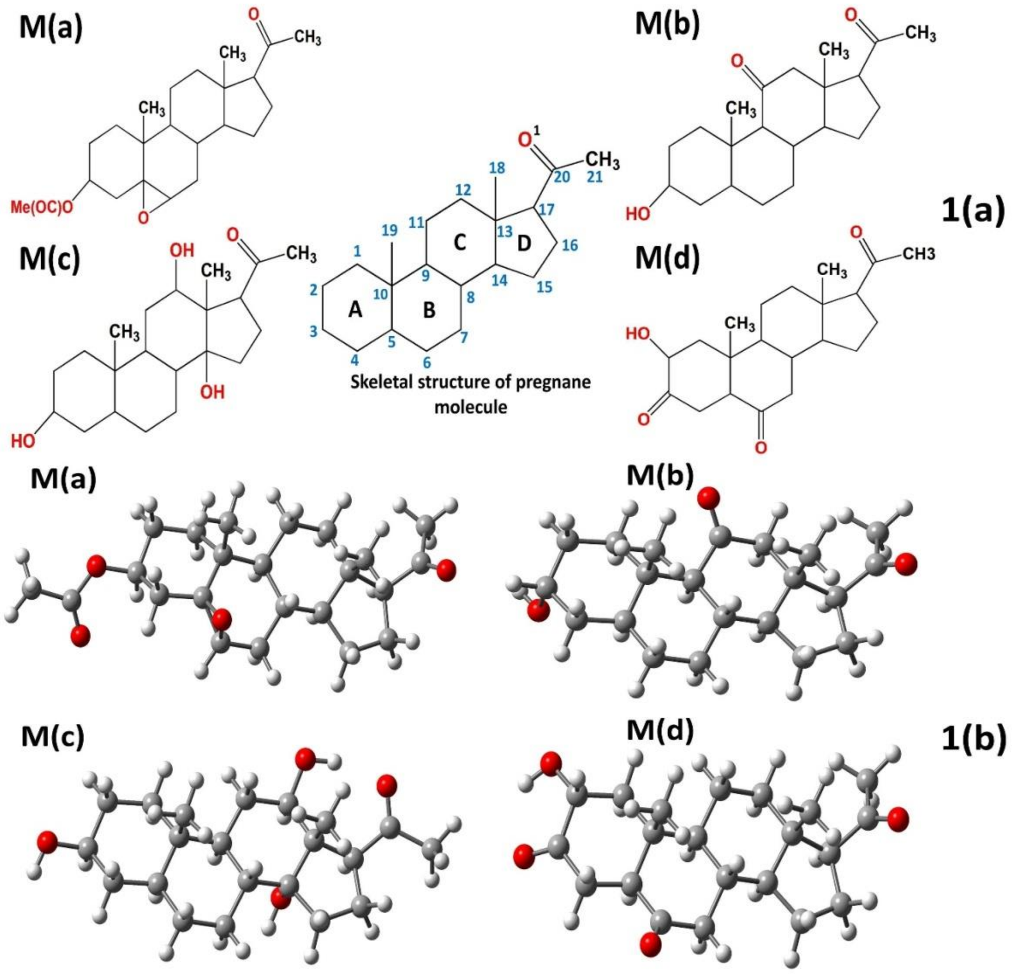

Figure 1: (a) The chemical structure of selected four pregnane derivatives with atomic numbering scheme (b) Optimized structure for M(a) – M(d)

Neha Kumari & Rajni Kant

Table 1: Crystallographic details of CSD structures (M(a) to M(d)).

Molecule	M(a)	M(b)	M(c)	M(d)
CCDC code	BIZPAC	HXPRDO	LOSKAG	RAFSAU
Chemical formula	$C_{23}H_{34}O_4$	$C_{21}H_{32}O_3$	$C_{21}H_{34}O_4$	$C_{21}H_{30}O_4$
Crystal system	Orthorhombic	Orthorhombic	Monoclinic	Monoclinic
Space group	$P2_12_12_1$	$P2_12_12_1$	$P2_1$	$P2_1$
Radiation used	MoKα	MoKα	MoKα	CuKα
Temperature (K)	293	295	293	150
Cell parameters (□□, ^{0})	a = 6.296 b = 11.893 c = 27.940 α = 90 β = 90 γ = 90	a = 7.372 b = 13.561 c = 18.493 α = 90 β = 90 γ = 90	a = 6.136 b =12.147 c = 12.759 α = 90 β = 101.51 γ = 90	a = 7.338 b= 10.170 c = 12.287 α = 90 β = 102.94 γ = 90
Unit cell volume ($Å^3$)	2091.90	1848.78	931.94	893.62
Z	4	4	2	2
R-factor (%)	4.14	6.30	4.81	5.96

The rings A, B & C exist in *chair* conformation while the ring D adopts *half chair* conformation except M(b) where it adopts an *envelope* conformation. The asymmetric parameters (ΔC_s & ΔC_2) for each structure were computed and are presented below:

Ring	BIZPAC M(a)	HXPRDO M(b)	LOSKAG M(c)	RAFSAU M(d)
A	ΔC_s = 8.64 ΔC_2 = 0.87	ΔC_s = 1.42 ΔC_2 = 3.75	ΔC_s =1.31 ΔC_2 =1.69	ΔC_s =0.57 ΔC_2= 6.01
B	ΔC_s = 10.68 ΔC_2= 15.98	ΔC_s = 1.23 ΔC_2 = 1.21	ΔC_s = 2.20 ΔC_2= 2.08	ΔC_s = 2.13 ΔC_2 = 1.83
C	ΔC_s = 2.29 ΔC_2 = 4.86	ΔC_s = 4.51 ΔC_2 = 4.15	ΔC_s = 2.52 ΔC_2 = 3.50	ΔC_s = 4.54 ΔC_2 = 1.78
D	ΔC_s= 13.38 ΔC_2 = 6.56	ΔC_s = 7.20 ΔC_2 =15.51	ΔC_s = 7.81 ΔC_2 = 12.39	ΔC_s = 2.09 ΔC_2 = 15.02

The optimized structures of [M(a-d)] are shown in Figure 1b. The average C-C ring bond lengths and that of the endocyclic bond angles in rings A, B and C are very close to their standard value [23]. The average value of bond angles in ring D (103.6^0) is significantly low as compared to the standard value of 109.6^0 [23].

3.2 Frontier molecular orbitals Analysis

The HOMO and LUMO plays a crucial role in determining the chemical behavior of a molecule. The LUMO acts as an electrophile, while the HOMO serves as a nucleophilic electron donor. A pictorial representation of frontier molecular orbitals and their respective energy gap values are reflected in Figure 2. The HOMO in M(a) is localized over the carboxylic group and the LUMO is concentrated over the acetyl group and partially on the ring D. The HOMO in M(b) shows a uniform spread over the entire molecule, while the LUMO is over ring C, D and the acetyl moiety. Further, the HOMO in M(c) is localized partially over the hydroxy and acetyl groups while the LUMO is over ring D and the acetyl group to some extent. The HOMO-LUMO energy gap range (5.59 and 6.06 eV), indicates stable characteristics for all the molecules. The chemical reactivity order in all the four molecules goes as M(c) > M(a) > M(b) > M(d).

3.3 Global chemical reactivity descriptor (GCRD)

The analysis of GCRD indicates that the molecules are kinetically stable with chemical hardness and chemical softness lying in the range: 2.79-3.03 eV and 0.16-0.71 $(eV)^{-1}$, respectively. The classification of organic molecules on the basis of electrophilicity index (ω) is termed as strong, moderate and weak electrophiles, with $\omega > 1.5$ eV, $0.8 < \omega < 1.5$ eV and $\omega < 0.8$ eV, respectively [24]. In the present case, the order of increasing electrophilic nature is M(a) > M(b) > M(c) > M(d) [25]. The GCRD values as obtained for each molecule are presented below:

Parameters	M(a)	M(b)	M(c)	M(d)
E_{HOMO}	-7.01	-6.80	-6.65	-6.86
E_{LUMO}	-1.41	-1.08	-1.06	-0.80
ΔE_g	5.60	5.72	5.59	6.06
$I = -E_{HOMO}$	7.01	6.80	6.65	6.86
$A= -E_{LUMO}$	1.41	1.08	1.06	0.80
$X =-\mu$	4.21	3.94	3.85	3.83
$\mu = -(I-A)/2$	-4.21	-3.94	-3.85	-3.83
$\eta = (I-A)/2$	2.83	2.86	2.79	3.03
$\sigma\ (eV)^{-1} = 1/2\eta$	0.71	0.17	0.17	0.16
$\omega = (I-A)/2$	3.16	2.71	2.65	2.42
$\Delta N_{max} = -\mu/\eta$	1.50	1.37	1.37	1.26

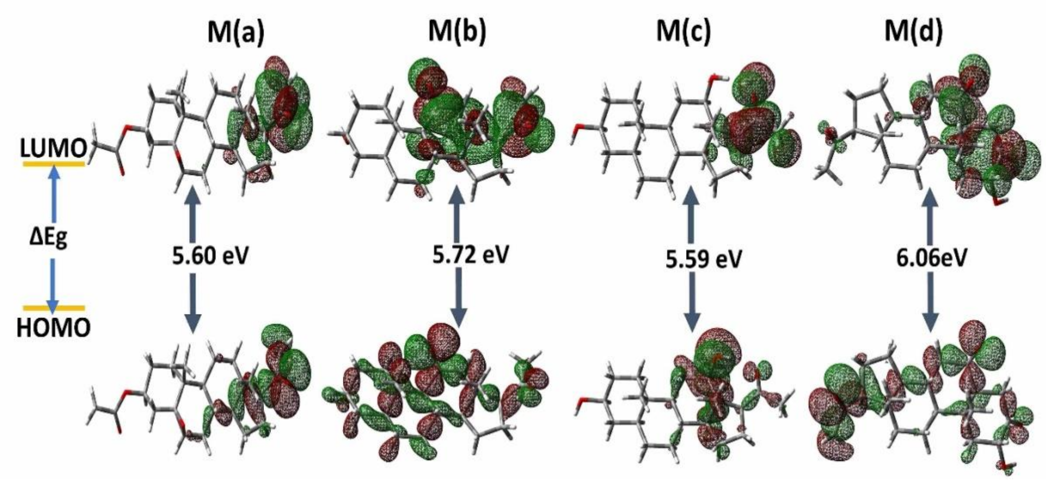

Figure 2: HOMO – LUMO energy gap for M(a) – M(d)

3.4 Molecular electrostatic potential (MESP)

The molecular electrostatic potential (MESP) helps in identifying reactive sites for electrophilic and nucleophilic attacks in chemical reactions, hydrogen bond interactions, and biological contexts. To identify suitable sites for nucleophilic and electrophilic attacks in all the pregnane molecules, the MESP maps have been plotted using the B3LYP/6-311++G(d,p) basis set (Figure 3). The surface regions are color-coded as red < orange < yellow < green < blue. The positive region is localized on the H atoms of the hydroxy group in case of M(b) and M(c), respectively, and that of the hydrogen atoms of ring B in case of M(d). The electronegative region (red) is concentrated around the oxygen atoms of carbonyl and hydroxy groups attached at various positions in each structure. The slightly electron-rich areas, represented as yellow in color, are close to red regions. The red region denotes the active sites of all molecules, which, in turn, denotes their possible sites for the biological activity.

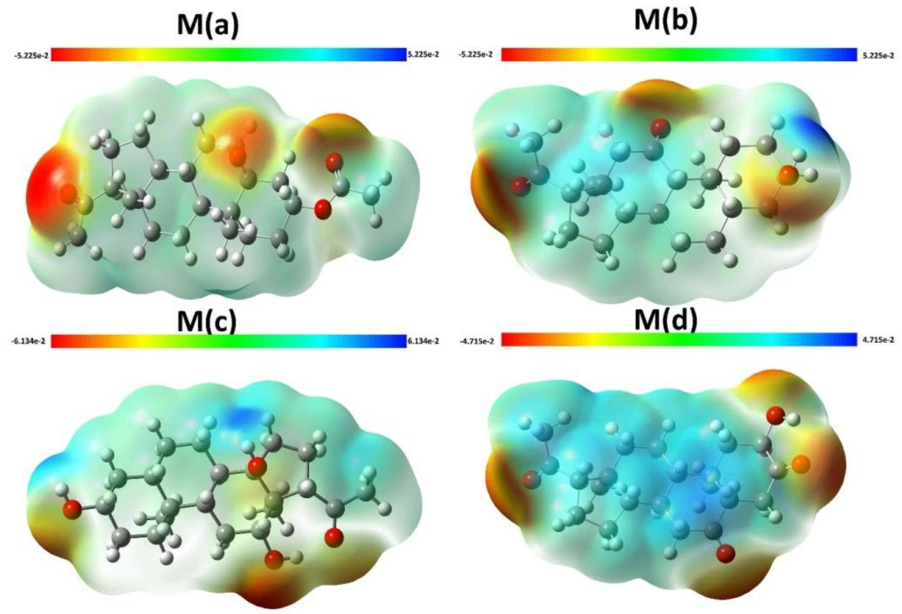

Figure 3: MESP maps for M(a) – M(d)

3.5 ELF and LOL maps

The electron localization function (ELF) and the localized orbital locator (LOL) are essential tools for analyzing the electron distribution within a molecule. ELF, denoted by τ(r), measures the probability of finding an electron pair in a specific region, with values ranging from 0.0 - 1.0 [26]. The ELF values (< 0.5) suggest electron delocalization; while (> 0.5-1.0) indicate regions with localized bonding or nonbonding electrons. In the ELF map, it can be seen that electrons are highly localized (red regions) around C-C atoms and C-H atoms in all the molecules under study. The elevated ELF values in red suggest strongly localized electrons surrounding the C-H atoms. The delocalized electron cloud density surrounding some carbon atoms is depicted by blue color with low ELF values. The LOL, denoted by η(r), measures electron localization but focuses on the gradients of localized orbitals (Figure 4a) [27]. High LOL values (> 0.5) indicate regions where electron density is dominated by localized electrons, such as in covalent bonds, lone pairs, or nuclear shells [28]. In the LOL plot, the central region of the hydrogen atom is white as the electron density exceeds the upper limit (0.8) of the color scale (Figure 4b). The majority of the covalent region is present between C-C atoms and C-H atoms, as indicated by the red color in both the maps. The blue circles around a few carbon nuclei show the electron depletion region between the inner shell and valence shell.

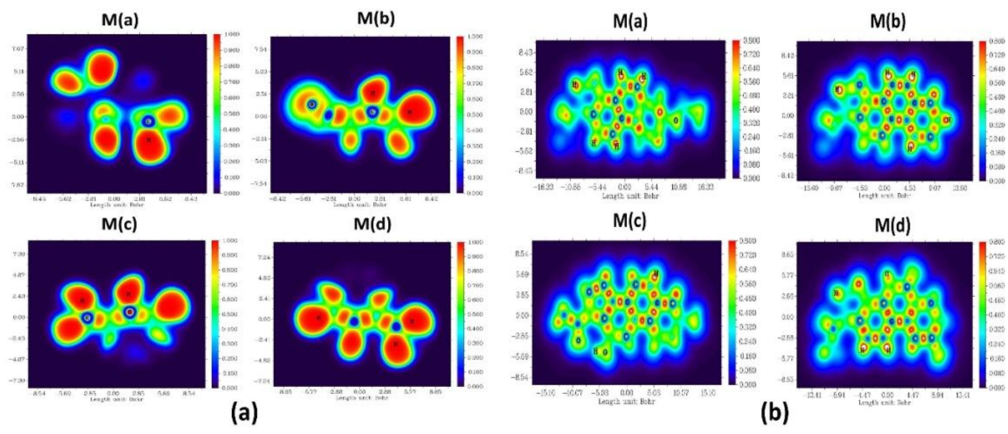

Fig. 4 (a) ELF and (b) LOL map for M(a) – M(d)

Neha Kumari & Rajni Kant

3.6 Hirshfeld surface analysis, fingerprint plots and crystal void analysis

Figure 5 shows the Hirshfeld surface of all molecules plotted over d_{norm}. The dark red spots on d_{norm} plot signify short intermolecular interactions, whereas lighter red dots indicate weaker interatomic interactions. The small red spots on the d_{norm} plots in M(a) indicate two types of C–H…O interactions {(C1–H1B…O) and C21–H21C…O1} while the dark red spots in molecule (M(b), M(c) and M(d)) reveals the presence of O–H...O intermolecular interactions. The faded color spot in case of M(b) confirms the presence of C–H…O interaction. The shape-index map, an indicator for the identification of π–π stacking, reveals the absence of π–π stacking interactions. However, the van der Waals forces have a significant impact on the crystal structure's ability to maintain its packing configuration in a stable state.

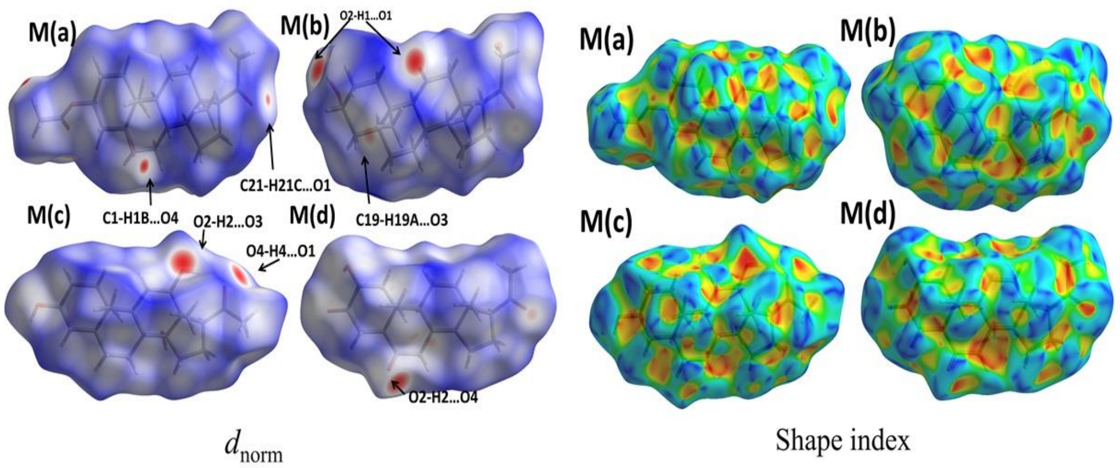

Figure 5: d_{norm} and shape-index maps for M(a) – M(d)

The analysis of the fingerprint plot reveals that the contribution of H....H interactions is dominant, with a respective contribution of 74.4%, 79.7%, 79.9% and 65.8%, respectively, for M(a-d). The O...H/H...O interactions emerge as the second most significant contributors in the crystal packing. Crystal Explorer 21.5 software [29] has been used to calculate the crystal voids in all molecules M(a-d) with void volume percentage being 15.35%, 13.40%, 12.87% and 11.32%, respectively. This indicates that M(d) exhibits better mechanical strength as compared to the other derivatives.

3.7 Molecular docking

Estrogen receptor beta (ERβ), a member of the nuclear receptor super family, is a key regulator of estrogen signaling with distinct tissue distribution and functional roles compared to estrogen receptor alpha (ERα). Research suggests that ERβ plays a crucial role in mediating estrogen's effects on diverse physiological processes such as cell proliferation, differentiation, inflammation, and neuroprotection [30-32]. Targeting ERβ with selective agonists or antagonists offers the potential for tissue-specific interventions, providing opportunities for developing novel therapies with improved efficacy and safety profiles.

The three-dimensional binding interaction of all molecules and the standard drug (fluoxymestreone), at the active site of the protein Estrogen receptor beta (1qkm) is shown in Figure 6. The various parameters of protein-ligand binding interactions are given in Table 2.

In the complex between M(a) and ERβ, several stabilizing interactions contribute to the compound's stability (Table 2). One conventional hydrogen bond is formed between the nitrogen atom of residue ARG346 and the oxygen atom of the ligand (M(a)) at a distance of 2.00 Å. Additionally, hydrophobic interactions, characterized as alkyl and π-alkyl, have been identified. These include interactions between the carbon atoms of PRO277, ARG346, VAL338, LYS401, and HSD279, and various regions of the ligand M(a), with distances ranging from 3.57 Å to 5.31 Å, respectively.

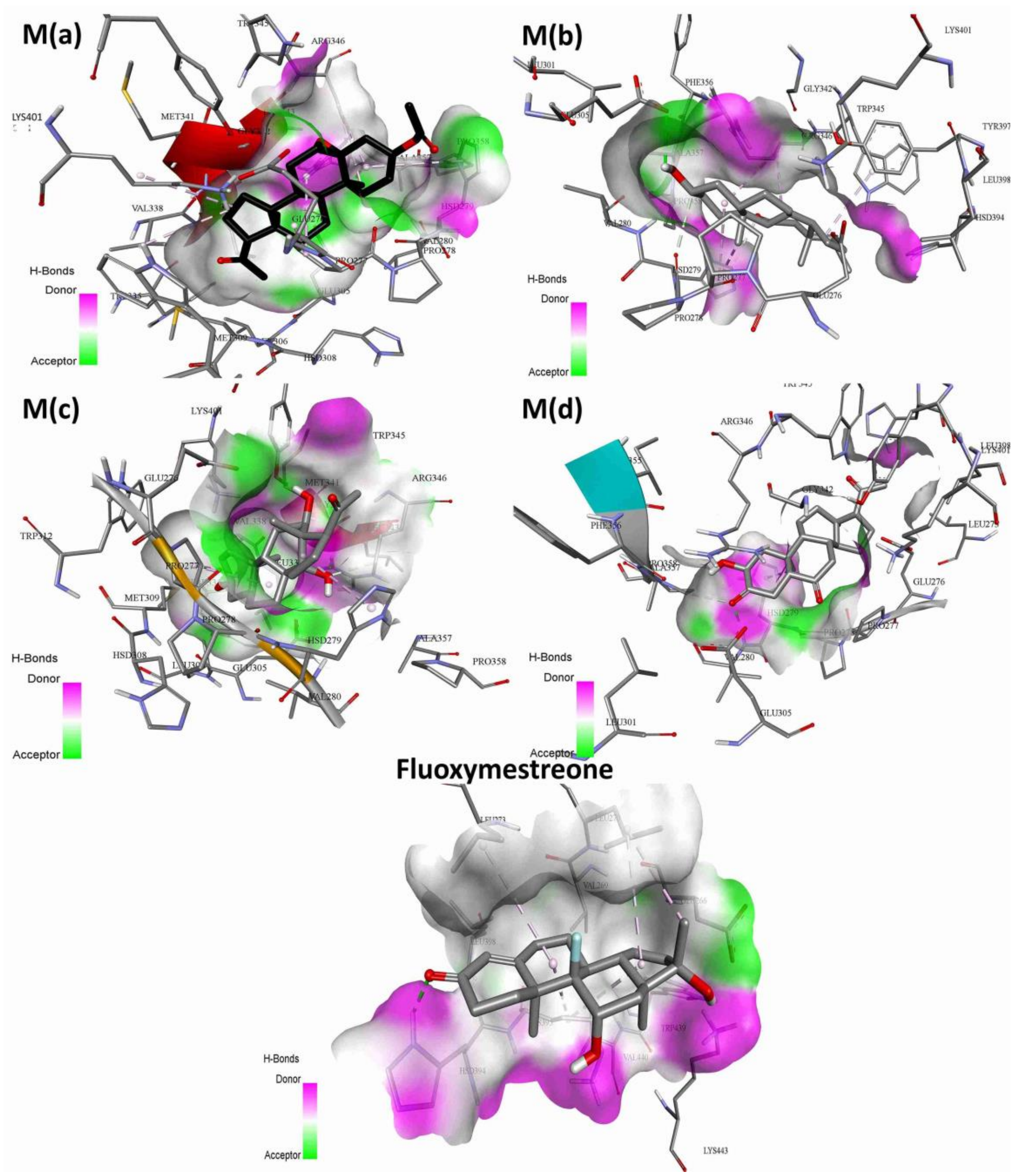

Figure 6: Protein-ligand interaction sites of M(a) – M(d) with 1qkm.

Table 2: Binding energy, different interactions, distances, bonding types of all molecules and fluoxymestreone with ERβ

Inhibitor	Binding energy (kcal/mol-¹)	Active site residue	Distance (Å)	Bonding	Bonding Types
M(a)	-9.3	ARG346 [NH…O]	2.00	HB	Conventional HB
		PRO277 [C…π]	4.41	Hydrophobic	Alkyl
		PRO277 [C…π]	3.57	Hydrophobic	Alkyl
		ARG346 [C…π]	5.31	Hydrophobic	Alkyl
		VAL338 [π…C]	5.00	Hydrophobic	Alkyl
		LYS401 [π…C]	4.55	Hydrophobic	Alkyl
		ARG346 [C…π]	5.08	Hydrophobic	Alkyl
		HSD279 [C…π]	5.22	Hydrophobic	π-Alkyl

Neha Kumari & Rajni Kant

M(b)	-8.6	GLU305 [O…H	2.53	HB	Conventional HB
		HSD279 [H…O]	3.47	HB	Carbon HB
		PRO278 [O…H]	3.35	HB	Carbon HB
		HSD279 [π…C]	3.83	Hydrophobic	π-Sigma
		ARG346 [C…π]	5.18	Hydrophobic	Alkyl
		ARG346 [C…π]	5.06	Hydrophobic	Alkyl
		HSD279 [C…π]	5.20	Hydrophobic	π-Alkyl
		TRP345 [C…π]	4.75	Hydrophobic	π-Alkyl
M(c)	-8.5	ARG346 [NH…O]	2.18	HB	Conventional HB
		TYR397 [O…H]	2.06	HB	Conventional HB
		ARG346 [H…O]	2.82	HB	Carbon HB
		PRO277 [C…π]	4.09	Hydrophobic	Alkyl
		PRO277 [C…π]	3.79	Hydrophobic	Alkyl
		HSD279 [C…π]	5.37	Hydrophobic	π-Alkyl
M(d)	-7.9	VAL280 [NH…O]	1.84	HB	Conventional HB
		PRO358 [O…H]	3.54	HB	Carbon HB
		HSD279 [C…π]	3.12	Hydrophobic	π-Sigma
Fluoxyme streone	-6.9	HSD394 [NH…O]	2.26	HB	Conventional HB
		LEU270 [C…π]	4.76	Hydrophobic	Alkyl
		LEU273 [C…π]	4.86	Hydrophobic	Alkyl
		LYS395 [C…π]	5.09	Hydrophobic	Alkyl
		LYS395 [C…π]	4.46	Hydrophobic	Alkyl
		LEU270 [π…C]	4.30	Hydrophobic	Alkyl

In the complex formed between M(b) and ERβ, some conventional hydrogen bonds have been observed between the oxygen atoms of GLU305, HSD279 and PRO278, and the ligand M(b), with distances ranging from 2.53 Å to 3.47 Å. Additionally, hydrophobic interactions, classified as π-sigma and π-alkyl, are identified between the carbon atoms of HSD279, ARG346, and TRP345, and M(b), with distances ranging from 3.83 Å to 5.20 Å. In the complex between M(c) and ERβ, the conventional hydrogen bonds are formed between the nitrogen and oxygen atoms of ARG346 and TYR397, respectively, with distances of 2.18 Å and 2.06 Å. Additionally, hydrophobic interactions, characterized as alkyl and π-alkyl, are identified between the carbon atoms of PRO277, HSD279, and the ligand M(c), with distances ranging from 3.79 Å to 5.37 Å.

Table 3. Comparison of the binding score of ERβ with pregnane structures and other ERβ modulators

S.No.	Inhibitors	Binding energy (kcal/mol^{-1})
1.	5β,6β-Epoxy-20-oxopregnan-3β-yl acetate	-9.3
2.	3α-Hydroxy-5α-pregnane-11,20-dione	-8.6
3.	3β,1β,14α-Trihydroxypregnan-20-one	-8.5
4.	2α-hydroxy-5α-pregnane-3,6,20-trione	-7.9
5.	Fluoxymestreone	-6.9
6.	Tamoxifen	-6.6
7.	Toremifene	-6.8
8.	Raloxifene	-7.7
10.	Mifepristone	-5.8

Similarly, in the complex between M(d) and ERβ, a combination of hydrogen bond and hydrophobic interactions contributes to the stability of the compound. Conventional hydrogen bonds are formed between the nitrogen and oxygen atoms of VAL280 and PRO358, respectively, with distances of 1.84 Å and 3.54 Å. Additionally, hydrophobic interactions, characterized as π-sigma, are identified between the carbon atoms of HSD279 and the M(d) ligand, with distances of 3.12 Å.

In the complex formed between fluoxymestreone and ERβ, conventional hydrogen bonds exist between the nitrogen and oxygen atoms of HSD394 and LEU270, respectively, with distances of 2.26 Å and 4.76 Å. Besides, the hydrophobic interactions, characterized as alkyl, exist between the carbon atoms of LEU270, LEU273, and LYS395, and the fluoxymestreone ligand, with distances ranging from 4.30 Å - 5.09 Å. The binding score of ERβ has been found comparable with several known ERβ modulator including, Tamoxifen, Toremifene, Raloxifene and Mifepristone [33], and the results are presented in Table 3. The comparison leads to the conclusion that the binding energy score in case of M(a-d) is better as compared to some analogous ERβ modulators. The presence of multiple favorable interactions in pregnane and ERβ complexes indicates a potentially stronger or more selective binding to ERβ, which may enhance therapeutic efficacy. Therefore, these inhibitors merit further investigation as promising alternatives or improvements to fluoxymestreone and other ERβ modulators in the context of ERβ-targeted therapies.

CONCLUSIONS

The optimized geometrical parameters closely align with the single crystal X-ray data. The analysis of HOMO–LUMO orbitals reveals the chemical stability of all molecules. The high electrophilicity index (ω) for M(a) (3.16 eV) confirms its ability to have better biological activity. The Hirshfeld surface reveals the presence of C–H…O and O–H…O intermolecular hydrogen bonding in the crystal packing. The highest contribution of H–H contacts in all molecules reveals the significance of van der Waal's interactions. The molecular docking study reveals that M(a) has good anti-cancer activity as compared to other pregnane derivatives and Erβ modulators.

Acknowledgement

The corresponding author Rajni Kant is thankful to the University of Jammu for the subscription of Licensed access of Cambridge Structure Database (*version: 2023*) at the Department of Physics, University of Jammu.

Funding

No specific grants or funding organizations from the public, commercial, or non-profit sectors provided financial support for this study.

Declaration

The authors declare that they have no known competing financial interests or personal relationships that could have appeared to influence the work reported in this paper.

Conflict of interest

The authors of this manuscript have no conflict of interest to declare.

REFERENCES

[1] Shen, Y., Burgoyne, D.L., 2002. Efficient synthesis of IPL576, 092: a novel anti-asthma agent. The Journal of Organic Chemistry, 67(11) 3908-3910. https://doi.org/10.1021/jo0108717.

[2] Sethi, A., Maurya, A., Tewari, V., Srivastava, S., Faridi, S., Bhatia, G., Khan, M.M., Khanna, A.K., Saxena, J.K., 2007. Expeditious and convenient synthesis of pregnanes and its glycosides as potential anti-dyslipidemic and anti-oxidant agents. Bioorganic & medicinal chemistry, 15(13) 4520-4527. https://doi.org/10.1016/j.bmc.2007.04.022.

[3] Cheng, W., Ren, J., Huang, Q., Long, H., Jin, H., Zhang, L., Liu, H., van Ofwegen, L., Lin, W., 2016. Pregnane steroids from a gorgonian coral Subergorgia suberosa with anti-flu virus effects. Steroids, 108, 99-104. https://doi.org/10.1016/j.steroids.2016.02.003.

[4] Huang, L.J., Chen, S.R., Yuan, C.M., Gu, W., Guo, B.J., Wang, Y.T., Wang, Y., Hao, X.J., 2017. C21-steroidal pregnane sapogenins and their derivatives as anti-inflammatory agents. Bioorganic & Medicinal Chemistry, 25(13) 3512-3524. https://doi.org/10.1016/j.bmc.2017.04.045.

[5] Sethi, A., Singh, R.P., Yadav, N., Banerjee, M., 2018. Synthesis, spectroscopic analysis (FT-IR, UV and NMR) and DFT analysis of novel prodrugs of pregnane, their apoptotic activity in cervical cancer cell

lines. Journal of Molecular Structure, 1166, 54-62. https://doi.org/10.1016/j.molstruc.2018.04.009.

[6] Alanzi, A.R., Parvez, M.K., Al-Dosari, M.S., 2023. Structure-based virtual identification of natural inhibitors of SARS-CoV-2 and its Delta and Omicron variant proteins. Future Virology, 18(7) 421-438. https://doi.org/10.2217/fvl-2022-0184.

[7] McLindon, L.A., James, G., Beckmann, M.M., Bertolone, J., Mahomed, K., Vane, M., Baker, T., Gleed, M., Grey, S., Tettamanzi, L., Mol, B.W.J., 2023. Progesterone for women with threatened miscarriage (STOP trial): a placebo-controlled randomized clinical trial. Human Reproduction, 38(4) 560-568. https://doi.org/10.1093/humrep/dead029.

[8] Maguire, J.L., Mennerick, S., 2024. Neurosteroids: mechanistic considerations and clinical prospects. Neuropsychopharmacology, 49 (1) 73-82. https://doi.org/10.1038/s41386-023-01626-z.

[9] Chang-Qing, Y., Jie, L., Shi-Qi, Z., Kun, Z., Zi-Qian, G., Ran, X., Hui-Meng, L., Ren-Bin, Z., Gang, Z., Da-Chuan, Y., Chen-Yan, Z., 2020. Recent treatment progress of triple negative breast cancer. Progress in biophysics and molecular biology, 151, 40-53. https://doi.org/10.1016/j.jep.2021.114581.

[10] Wang, Y., Shen, S.Y., Liu, L., Zhang, X.D., Liu, D.Y., Liu, N., Liu, B.H., Shen, L., 2022. Jolkinolide B inhibits proliferation or migration and promotes apoptosis of MCF-7 or BT-474 breast cancer cells by down regulating the PI3K-Akt pathway. Journal of Ethnopharmacology, 282, 114581. https://doi.org/10.1016/j.jep.2021.114581.

[11] Chen, P., Li, B., Ou-Yang, L., 2022. Role of estrogen receptors in health and disease. Frontiers in endocrinology, 13, 839005. https://doi.org/10.3389/fendo.2022.839005

[12] Pinto, R.M., Salvador, J.A., Paixão, J.A., 2008. 5β, 6β-Epoxy-17-oxoandrostan-3β-yl acetate and 5β, 6β-epoxy-20-oxopregnan-3β-yl acetate. Acta Crystallographica Section C: Crystal Structure Communications, 64(5) o279-o282. https://doi.org/10.1107/S0108270108009621.

[13] Midgley, J.M., Whalley, W.B., Ferguson, G., Marsh, W.C., 1978. Conformational studies. Part 11. Crystal and molecular structure of the anaesthetic, 3α-hydroxy-5α-pregnane-11, 20-dione. Journal of the Chemical Society, Perkin Transactions 2, (10) 1042-1044. https://doi.org/10.1039/P29780001042.

[14] Shi, H., Li, Y., 2009. 3β, 12β, 14α-Trihydroxypregnan-20-one. Acta Crystallographica Section E: Structure Reports Online, 65(5) o1102-o1102. https://doi.org/10.1107/S1600536809013853.

[15] Marek, A., Klepetářová, B., Elbert, T., 2011. The introduction of a double bond on the steroid skeleton–The preparation of enol silyl ether derivatives from vicinal diols. Collection of Czechoslovak Chemical Communications, 76(5), 443-456. https://doi.org/10.1135/cccc2010145.

[16] Becke, A.D., 1992. Density-functional thermochemistry. I. The effect of the exchange-only gradient correction. The Journal of chemical physics, 96(3) 2155-2160. https://doi.org/10.1063/1.464913

[17] Becke, A.D., 1988. Density-functional exchange-energy approximation with correct asymptotic behavior. Physical review A, 38(6) 3098. https://doi.org/10.1103/PhysRevA.38.3098.

[18] Frisch, M.J., Trucks, G. W., Schlegel, H. B., Scuseria, G. E., Robb, M. A. Cheeseman, J. R., Scalmani, G., Barone, V., Mennucci, B., Petersson, G.A., Nakatsuji, H., Gaussian 09, Revision E.01.

[19] Lu, T., Chen, F., 2012. Multiwfn: A multifunctional wave function analyzer. Journal of computational chemistry, 33(5) 580-592. https://doi.org/10.1002/jcc.22885.

[20] Spackman, P.R., Turner, M.J., McKinnon, J.J., Wolff, S.K., Grimwood, D.J., Jayatilaka, D., Spackman, M.A., 2021. Crystal Explorer: a program for Hirshfeld surface analysis, visualization and quantitative analysis of molecular crystals. Journal of Applied Crystallography, 54(3) 1006-1011.

https://doi.org/10.1107/S1600576721002910.

[21] Morris, G.M., Huey, R., Lindstrom, W., Sanner, M.F., Belew, R.K., Goodsell, D.S., Olson, A.J., 2009. AutoDock4 and AutoDockTools4: Automated docking with selective receptor flexibility. Journal of computational chemistry, 30(16), 2785-2791. https://doi.org/10.1002/jcc.21256

[22] BIOVIA discovery studio visualizer. Software version, **20**, 779 (2016).

[23] Soumya, S., Joe, I.H., 2021. A combined experimental and quantum chemical study on molecular structure, spectroscopic properties and biological activity of anti-inflammatory Glucocorticosteroid drug, Dexamethasone. Journal of Molecular Structure, 1245, 130999. https://doi.org/10.1016/j.molstruc.2021.130999

[24] Janani, S., Rajagopal, H., Muthu, S., Aayisha, S., Raja, M., 2021. Molecular structure, spectroscopic (FT-IR, FT-Raman, NMR), HOMO-LUMO, chemical reactivity, AIM, ELF, LOL and Molecular docking studies on 1-Benzyl-4-(N-Boc-amino) piperidine. Journal of Molecular Structure, 1230, 129657. https://doi.org/10.1016/j.molstruc.2020.129657

[25] Parthasarathi, R., Subramanian, V., Roy, D.R., Chattaraj, P.K., 2004. Electrophilicity index as a possible descriptor of biological activity. Bioorganic & medicinal chemistry, 12(21), pp.5533-5543. https://doi.org/10.1016/j.bmc.2004.08.013

[26] Silvi, B., Savin, A., 1994. Classification of chemical bonds based on topological analysis of electron localization functions. Nature, 371(6499) 683-686. https://doi.org/10.1038/371683a0.

[27] Jacobsen, H., 2008. Localized-orbital locator (LOL) profiles of chemical bonding. Canadian Journal of Chemistry, 86(7) 695-702. https://doi.org/10.1139/v08-052.

[28] Spackman, M.A., McKinnon, J.J., 2002. Fingerprinting intermolecular interactions in molecular crystals. Cryst Eng Comm, 4(66) 378-392. https://doi.org/10.1039/B203191B

[29] Turner, M.J., McKinnon, J.J., Jayatilaka, D., Spackman, M.A., 2011. Visualisation and characterization of voids in crystalline materials. Cryst Eng Comm, 13(6) 1804-1813. https://doi.org/10.1039/C0CE00683A.

[30] Weihua, Z., Saji, S., Mäkinen, S., Cheng, G., Jensen, E.V., Warner, M., Gustafsson, J.Å., 2000. Estrogen receptor (ER) β, a modulator of ERα in the uterus. Proceedings of the National Academy of Sciences, 97(11) 5936-5941. https://doi.org/10.1073/pnas.97.11.5936.

[31] Hartman, J., Edvardsson, K., Lindberg, K., Zhao, C., Williams, C., Ström, A., Gustafsson, J.A., 2009. Tumor repressive functions of estrogen receptor β in SW480 colon cancer cells. Cancer research, 69(15) 6100-6106. https://doi.org/10.1158/0008-5472.CAN-09-0506

[32] Nilsson, S., Koehler, K.F., Gustafsson, J.Å., 2011. Development of subtype-selective oestrogen receptor-based therapeutics. Nature reviews Drug discovery, 10(10), 778-792. https://doi.org/10.1038/nrd3551

[33] Mukherjee, S., Majumder, D., 2009. Computational molecular docking assessment of hormone receptor adjuvant drugs: breast cancer as an example. Pathophysiology, 16(1), 19-29. https://doi.org/10.1016/j.pathophys.2008.12.001